NANO · MICRO small
www.small-journal.com

Highly-Directional, Highly-Efficient Solution-Processed Light-Emitting Diodes of All-Face-Down Oriented Colloidal Quantum Well Self-Assembly

*Hamed Dehghanpour Baruj, Iklim Bozkaya, Betul Canimkurbey, Ahmet Tarik Isik, Farzan Shabani, Savas Delikanli, Sushant Shendre, Onur Erdem, Furkan Isik, and Hilmi Volkan Demir**

Semiconductor colloidal quantum wells (CQWs) provide anisotropic emission behavior originating from their anisotropic optical transition dipole moments (TDMs). Here, solution-processed colloidal quantum well light-emitting diodes (CQW-LEDs) of a single all-face-down oriented self-assembled monolayer (SAM) film of CQWs that collectively enable a supreme level of IP TDMs at 92% in the ensemble emission are shown. This significantly enhances the outcoupling efficiency from 22% (of standard randomly-oriented emitters) to 34% (of face-down oriented emitters) in the LED. As a result, the external quantum efficiency reaches a record high level of 18.1% for the solution-processed type of CQW-LEDs, putting their efficiency performance on par with the hybrid organic-inorganic evaporation-based CQW-LEDs and all other best solution-processed LEDs. This SAM-CQW-LED architecture allows for a high maximum brightness of 19,800 cd m^{-2} with a long operational lifetime of 247 h at 100 cd m^{-2} as well as a stable saturated deep-red emission (651 nm) with a low turn-on voltage of 1.7 eV at a current density of 1 mA cm^{-2} and a high J_{90} of 99.58 mA cm^{-2}. These findings indicate the effectiveness of oriented self-assembly of CQWs as an electrically-driven emissive layer in improving outcoupling and external quantum efficiencies in the CQW-LEDs.

1. Introduction

Semiconductor colloidal quantum wells (CQWs), alternatively nicknamed nanoplatelets (NPLs), having a quasi-two-dimensional structure with pure thicknesses, have emerged as an important class of nanocrystals (NCs).[1–4] Compared to their spherical counterparts, NPLs exhibit a narrow emission bandwidth due to their suppressed inhomogeneous broadening, extraordinarily large absorption cross-section owing to their giant oscillator strength, and highly suppressed Auger recombination thanks to their non-confined lateral dimensions.[3,4,13–16,5–12] These features have led to the fabrication of high external quantum efficiency (EQE) and high-color purity colloidal quantum well light-emitting diodes (CQW-LEDs) using hybrid organic-inorganic devices structures. For example, in the previous work of our group, we reported a high EQE value of 19.2% with a maximum brightness of 23 490 cd m^{-2} for the hybrid organic-inorganic inverted CQW-LEDs.[17] However, the efficiency of CQW-LEDs having only all-solution processed structures in their layers is still lagging far behind the state-of-the-art values obtained with evaporation-based devices.[11,18,19] Since the solution-processable architecture is relatively easier to fabricate and cheaper than the evaporation-based ones, achieving a high EQE from all-solution-processed LEDs is of great interest. Thus far, Kelestemur et al. reported the highest EQE of 9.92% with a maximum brightness of 46 000 cd m^{-2} for all-solution processed red-emitting CQW-LED.[11] However, this EQE value was insufficient to fulfill the industrial demands. The fundamental light-extraction efficiency limitation and exciton quenching of the zinc oxide (ZnO) layer impede the maximum EQEs to reach the state-of-the-art values in the case of all-solution processing.[17,20]

As a new strategy, we target to overcome the light extraction efficiency limitation by exploiting self-assembled monolayer (SAM) films of NPLs as an emissive layer (EML).[21–23] In this regard, NPLs are highly advantageous owing to their anisotropic transition dipole moments (TDMs).[21–23] The CQWs are from the family of anisotropic atomically flat, thin nano-emitters that

H. D. Baruj, I. Bozkaya, B. Canimkurbey, A. T. Isik, F. Shabani, S. Delikanli, O. Erdem, F. Isik, H. V. Demir
Department of Electrical and Electronics Engineering
Department of Physics
UNAM – Institute of Materials Science and Nanotechnology
Bilkent University
Ankara 06800, Turkey
E-mail: volkan@bilkent.edu.tr

B. Canimkurbey
Central Research Laboratory
Amasya University
Amasya 05100, Turkey

S. Delikanli, S. Shendre, H. V. Demir
LUMINOUS! Center of Excellence for Semiconductor Lighting and Displays
School of Electrical and Electronic Engineering
School of Physical and Mathematical Sciences
Nanyang Technological University
Singapore 639798, Singapore

The ORCID identification number(s) for the author(s) of this article can be found under https://doi.org/10.1002/smll.202206582.

DOI: 10.1002/smll.202206582

exhibit almost all in-plane (IP) TDMs.[13,22–27] Thus, an all-face-down ensemble film of CQWs can act as a highly anisotropic EML. The Fresnel equation suggests that, from the emitter point of view, the ray escape cone has an outcoupling angle of 30° to the surface normal.[13,22–24] Accordingly, the density of light inside the cone determines the intensity of extracted light. It has been reported that the ratio of optical power inside the cone is higher in a device with directional EML than in isotropic EML.[13,22,23,25–31]

To control the orientation of CQWs, many deposition methods such as inkjet printing,[32] evaporation depositions,[33] and self-assembly[23,30,34] have been introduced. Among them, the most feasible and practical technique that provides total control over a millimeter square or larger size film is the liquid-air interface self-assembly. The feasibility of this method on the deposition of SAM in an all-face-down configuration across a large-area and uniform film out of colloidal quantum wells has been reported previously by our group.[34] Self-assembly has indeed been used to deposit a large variety of two-dimensional nanocrystals ranging from CQWs to perovskites. In all of these previous reports, the self-assembly of these 2D-colloids has been usual in passive optical structures, where these nanocrystals are excited optically using an external light source. Thus far, such oriented self-assembly CQWs, or any other colloids for that matter into an active device has not been possible. Here, addressing the interaction issues of liquid-air interface self-assembly sub-phase with active device layers and creating a highly uniform monolayer film free of pinholes allowed us to obtain highly efficient devices fabricated using oriented CQWs.

In addition, self-assembly provides the lowest possible root-mean-square (RMS) roughness among the various deposition techniques yielding an RMS roughness comparable with the spherical nanocrystals.[17,35] The film roughness, especially the EML film roughness, is a deterministic factor in the efficiency of the devices.[9,17,36–38] The interlayer transfer of electrons occurs by the hopping process, which depends on the atomic-scale distance between layers and hence the roughness of EML.[2,39] Thus, self-assembled CQWs potentially make an excellent EML in an LED.

In this paper, we proposed and demonstrated a high-performance all-solution-processed CQW-LED having an all-face-down SAM film of CQWs as an EML through precise control over the liquid-air self-assembly for the first time. Our optimized device architecture is made of consecutive layers of indium tin oxide (ITO, 100 nm)/poly(ethylene dioxythiophene):polystyrene sulphonate (PEDOT:PSS, 30 nm)/poly (*N*,N9-bis(4-butyl phenyl)-N,N9-bis(phenyl)-benzidine) (p-TPD, 20 nm)/poly(9-vinyl carbazole) (PVK,10 nm)/CQWs /$Zn_{0.95}Mg_{0.05}O$(30 nm)/Al(100 nm). Using back-focal plane (BFP) imaging techniques on our all-face-down SAM film of CQWs, we measured TDMs direction (Θ) to be 92% in-plane (IP). Considering our device's structure, we calculated the outcoupling efficiency to be 34%, which is significantly higher than 22% of the conventional solution-processed structures with isotropic emitters as an EML and without any light extraction feature. Our SAM-CQW-LEDs reached an outstanding EQE of 18.1 with a high luminance level of 19 800 cd m^{-2} and a long lifetime of 247 h at 100 cd m^{-2} using ligand-exchanged CdSe/$Cd_{0.25}Zn_{0.75}S$ core/hot-injection shell (HIS) CQWs. These values are comparable to those of the best-reported organic-inorganic hybrid CQW-LEDs, state-of-the-art OLEDs, PeLEDs, and QLEDs. In this work, using the strategy of orienting our emitters in the active device architecture, we have therefore overcome the fundamental outcoupling efficiency limitations commonly encountered in conventional colloidal device structures.

2. Results and Discussion

In this study, we used high photoluminescence quantum yield (PLQY) core/hot-injection shell (HIS) NPLs previously developed by our group,[8,17,40] consisting of square-shaped cores with a gradient shell and oleic acid (OA) and oleylamine (OLA) ligands. The shell of $Cd_{0.25}Zn_{0.75}S$ was grown on the CdSe cores by adding the cadmium and zinc precursors at room temperature and continuously injecting the sulfur precursor at higher temperatures (the hot-injection method). Details of the synthesis procedures of CQWs are given in the Supporting Information. The outer shell structure ensures the confinement of the excitons inside the core region to impede nonradiative recombination by surface traps.[41] The gradient shell structure also provides a low lattice mismatch between the core and the outer shell, which reduces interface defects and nonradiative recombination. Finally, the outmost layer consists of OA and OLA ligands.[17,38] The role of these ligands is to allow for good solubility in the colloidal solution, which is a critical parameter for solution-processed fabrication techniques while passivating the surface defects. Thanks to their heterostructure, the obtained NPLs show a PLQY of 95% in the solution and 87% on the quartz substrate, which is the highest PLQY among all types of CQWs in the saturated deep-red color, with excellent chemical and optical stability.[13,14,17,40,42]

We employed these highly efficient CQWs in our LED structure as an active layer. Our LED structure consists of indium tin oxide (ITO, 100 nm)/poly(ethylene dioxythiophene):polystyrene sulphonate (PEDOT:PSS, 30 nm)/poly (*N*,N9-bis(4-butyl phenyl)-N,N9-bis(phenyl)-benzidine) (p-TPD, 20 nm)/poly(9-vinyl carbazole) (PVK, 10 nm)/CQWs (4 nm) /$Zn_{0.95}Mg_{0.05}O$(30 nm) /Al (100 nm). (see **Figure 1**a,b). All these layers were deposited using the spin-coating technique in dynamic mode except for the PVK layer, which was in static mode. The cross-sectional TEM image of the self-assembled CQW film-based device, profiled with its energy-dispersive X-ray spectroscopy (EDAX), shows all deposited layers in the device as provided in Figure 1a. The thickness of the CQW film obtained from TEM cross-section, marked with Cd and Se in its EDAX, in the device is ≈4.0 ± 0.5 nm, which matches the vertical thickness of a single CQW obtained from its TEM image presented in Figure S6 (Supporting Information). Therefore, this film thickness of the CQW ensemble, identified with the EDAX device profile to be as thin as an individual CQW, supports that this self-assembled layer has to have only face-down oriented CQWs (not a mixture of different orientations) and it has to be a monolayer of these face-down CQWs (not two or more layers). In addition, we show a zoomed-in high-resolution image of the self-assembled monolayer film of CQWs, which displays individual CQWs all with face-down orientation in Figure 1a. This image proves the successful deposition of a

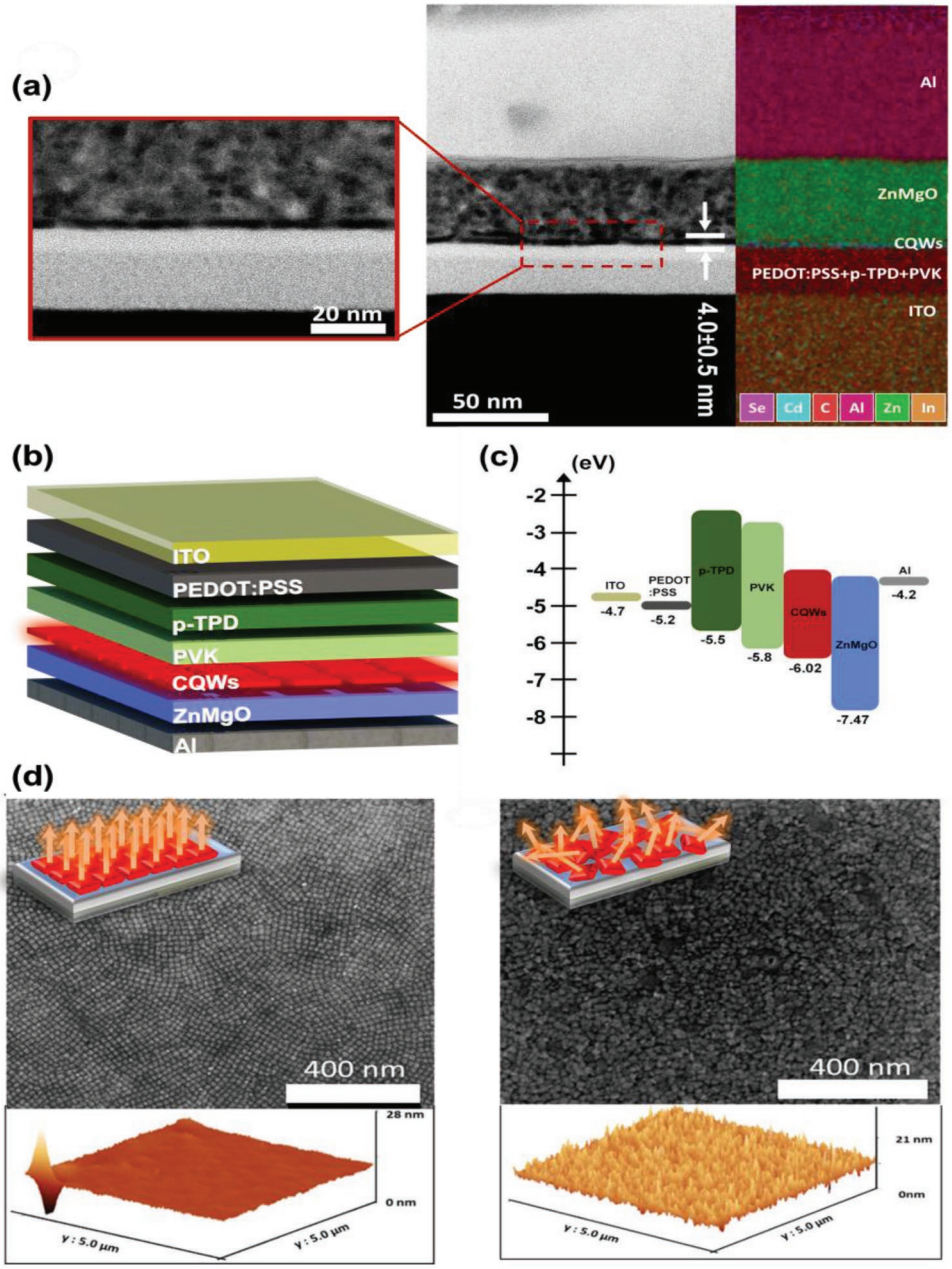

Figure 1. a) Transmission electron microscopy (TEM) cross-sectional image of the device containing the face-down oriented hot-injection shell (HIS) grown CQW SAM, marked with its energy-dispersive X-ray spectroscopy (EDAX) mapping. Using this EDAX-mapped TEM image (scale bar: 50 nm), the film thickness of these self-assembled CQWs in the device is measured to be ≈4.0 ± 0.5 nm, which matches the vertical thickness of a single individual CQW. A zoomed-in image of a monolayer self-assembled film of CQWs with all-face-down orientations is also presented with a scale bar of 20 nm. As direct evidence, these prove that the self-assembled CQWs are in face-down orientation and of only one monolayer. b) Schematic of the device structure and c) energy band diagram of the optimized structure. d) Scanning electron microscopy (SEM) image of the all-face-down self-assembled monolayer with its atomic force microscopy (AFM) scan (left-hand side). Inset: the schematic of all-face-down SAM film of NPLs on the device's layers. SEM image of the spin-casted film of NPLs with the corresponding AFM scan (right-hand side). Inset: the schematic of a spin-casted film of NPLs on the device's layers.

single monolayer film of CQWs with face-down orientation in the actual devices.

Here, in this device structure, we took advantage of both the high hole mobility provided by poly-TPD (1×10^{-4} cm^{-1} V^{-1} s^{-1}) and the deep highest-occupied-molecular-orbit (HOMO) energy level (–5.8 eV) provided by PVK. This bilayer structure accompanied by PEDOT:PSS provides a stepwise energy level alignment between ITO and EML (see Figure 1c). Moreover, as an electron transport layer (ETL), we used Mg-doped ZnO (5%) to diminish the exciton quenching.[12,43–45]

It is known that the direct contact of ZnO to NPLs quenches the emission due to the nonradiative energy transfer, but this

phenomenon is significantly suppressed by doping Mg in the ZnO structure.[43,45] To confirm this effect, we analyzed in-film PLQY of HIS NPLs on ZnO and $Zn_{0.95}Mg_{0.05}O$ layers. We found that in-solution PLQY of 95% for the NPLs dropped to 55% on ZnO and 64% on $Zn_{0.95}Mg_{0.05}O$. Therefore, this quenching limits the maximum achievable EQE based on the following relation.[17,20]

$$EQE = \eta_{out} \times r \times q \times \gamma \quad (1)$$

Here, η_{out} represents the extraction efficiency, r denotes the fraction of excitons with the probability of radiative recombination, q is the film PLQY, and γ gives the charge injection efficiency inside the device. Since the EQE and q are directly correlated, a decrease in q reduces the EQE. Here we conclude that utilizing the $Zn_{0.95}Mg_{0.05}O$ nanocrystals as an ETL is preferable to the ZnO nanocrystals in our devices. Moreover, the charge balance can be justified by checking the electronic and hole-only devices' current density versus voltage (J–V) curves. The J–V curve of the electron-only device fabricated by $Zn_{0.95}Mg_{0.05}O$ is closer to the hole-only device's J–V than the electron-only device manufactured by ZnO nanoparticles (see Figure S1, Supporting Information).

The successful deposition of a single all-face-down oriented SAM film of CQWs is also evident from the comparative SEM imaging provided in Figure 1d. Here we display a top-view image of a CQW-SAM film in contrast to that of spin-coated randomly-oriented CQW film. The appearance of a clean and neat mosaic-like texture observed only in the top-view image of the self-assembled film indicates the successful preparation of a monolayer of face-down CQW film. To achieve a highly efficient device using a single monolayer assembly of oriented NPLs, the film should be highly uniform when all face-down (see Figure 1d) but at the same time pinhole-free to avoid charge leakage. Such a monolayer film can be achieved by precise control using liquid-air self-assembly. In doing so, it is essential to prevent crack formation during the draining process, the pre-existed defects in the substrate, and the possible effects of subphases with the layers of the device. In this work, to be compatible with active device fabrication, we modified the liquid-air interface self-assembly approach our group previously developed to make passive film[34] and explored the applicability in the deposition of a highly uniform and pinhole-free all-face-down SAM film NPLs as an active film on top of the devices' layers. In this process, after coating the hole injection layer (HIL) and hole transport layers (HTLs), inside the N_2-filled glovebox, the substrates were moved into a Teflon container poured by the acetonitrile (ACN) subphase. Subsequently, 20 µL of NPL in hexane solution was dropped on the ACN from the edge of the container. They were dispersed across the surface of the subphase as soon as they fell on the ACN. After evaporation of hexane, a uniform all-face-down membrane of NPLs was obtained on top of the subphase. To transfer this film to the substrates, the ACN was drained through a needle from the bottom of the container, and the film sank onto the substrate coated with the PVK layer on the top. Note that for having a uniform film, the height of ACN on top of the substrate should be as low as possible to have the least amount of movement of the ensembled film while draining. Also, we have used silicon oil surfactant to compress the SAM membrane further and avoid crack and void formation during the deposition process due to capillary forces by the walls of the container.[34]

Figure 1c shows the scanning electron microscopy (SEM) image of the mosaic-like structure of the SAM film, which is highly uniform with a complete surface coverage of NPLs on top of HTL compared to the spin-casted film that is randomly oriented. Inset schematics also illustrate the difference in the architecture of the films deposited by self-assembly (all-face-down oriented) and spin-casting (randomly oriented), respectively, with their corresponding emission polarization. Also, the atomic force microscopy (AFM) measurements reveal the RMS roughness <1 nm for the SAM films and 2.4 nm for the spin-coated ones (see Figure 1c). These results imply that the orientation-controlled film yields the lowest possible surface roughness, which is comparable with that of spherical nanocrystal film. This reduction in film roughness of NPLs should increase the charge injection.

In addition, to check the potential effects of ACN solvent on the electronic properties of HTLs and HIL, we fabricated hole-only devices with the structure of ITO/PEDOT:PSS/p-TPD/PVK/NPLs/Al. The layers were deposited by spin-coating process except for Al which was deposited by thermal evaporation. In this device, after depositing the ITO/PEDOT:PSS/p-TPD/PVK layers, we placed the sample inside the ACN for 5 min and then baked it for 30 min at 90 °C. Finally, the NPLs were coated on the samples, followed by Al deposition. As shown in Figure S3 (Supporting Information), no apparent changes were detected in the hole-only device current density versus voltages (J–V) characteristics with and without drowning in ACN.

From the all-face-down SAM film, as shown schematically in Figure 1c, we expect to obtain directional emission compared to that of the random-oriented one. Since CQWs possess nearly all in-plane transition dipole moments, their all-face-down ensemble film should act as an anisotropic emissive film. To realize the direction of emission (Θ) of the deposited all-face-down single monolayer CQW film, we have used the back-focal plane (BFP) imaging technique. In this imaging, we found the ratio of the horizontal ($p_{\parallel}$) component to the sum of the horizontal and vertical ($p_{\perp}$) elements ($\Theta = p_{\parallel}/(p_{\parallel} + p_{\perp})$), which experimentally quantified the directionality of TDMs. Figure S7 (Supporting Information) illustrates the schematic of our BFP setup. In this experiment, spin-casted and single monolayer self-assembled films of NPLs on 200 µm thick quartz substrates were excited by a 400 nm laser, and a CCD camera took the back-focal plane images. **Figure 2**a,b shows the simulated intensity profile for fully in-plane (IP) and out-of-plane (OP) TDMs with the k_x-intensity diagrams for the p-polarized emission, given next to the images, respectively. The BFP images of self-assembled single monolayer and spin-coated samples with the k_x-intensity diagrams for the p-polarized emission are provided in Figure 2c,d. Using the intensity diagrams of fully IP, OP, and their fit to the self-assembled film's intensity diagram (see Figure 2c), we found Θ equal to 92%. By repeating the same process for the random-oriented samples (see Figure 2d), we found the Θ equal to 67% (see the SI for the measurement and simulation details). Scott et al.[23] reported Θ was 95% for all-face-down CdSe NPLs and Shendre et al.[13] found Θ of 91% for all-face-down CdSe/CdS@ CdZnS. Our measured Θ agrees

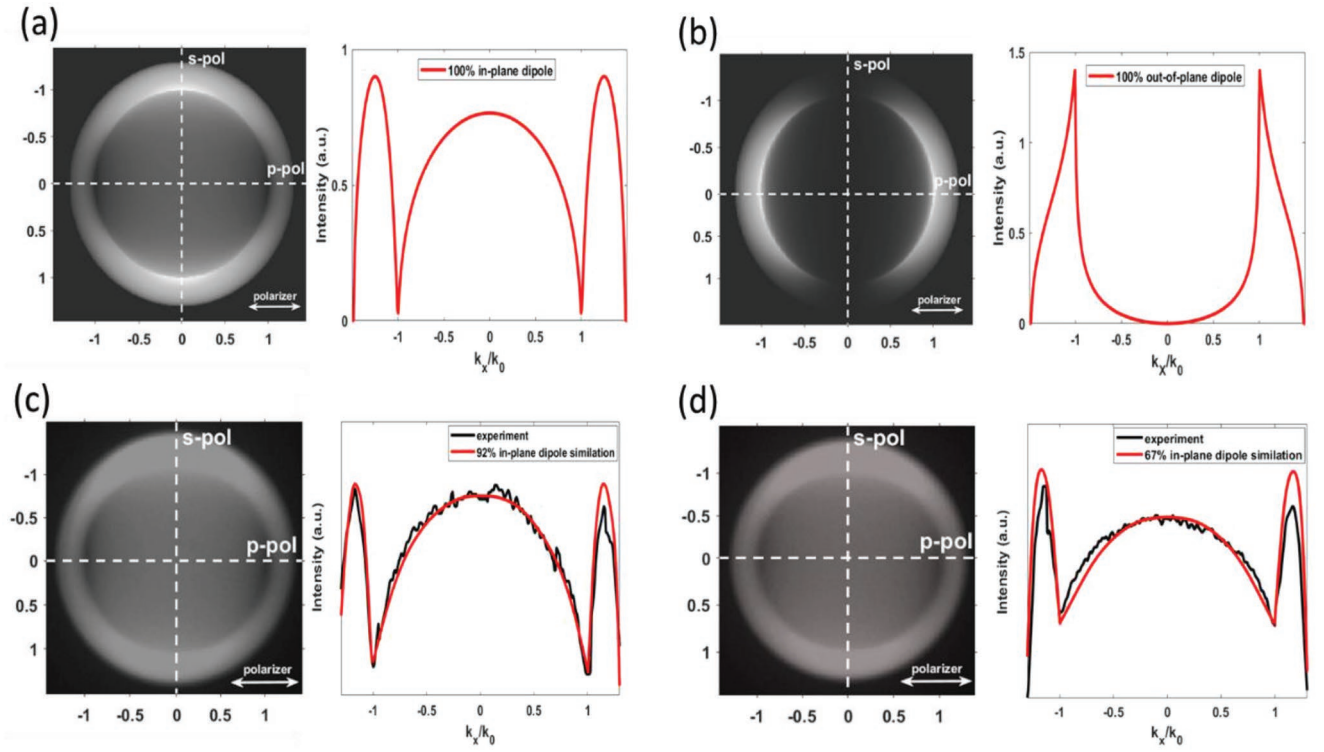

Figure 2. Emission profile and intensity diagrams of a) fully IP TDMs, b) full OP TDMs, c) self-assembled monolayer film on a quartz substrate with 92% IP TDMs fitting curve, and d) spin-casted film on a quartz substrate with 67% IP TDMs curve.

with these results in the literature. These results confirm that in the all-face-down SAM film, a bright plane is directed toward the glass substrate.

Based on the measured Θ values, we calculated the light outcoupling efficiencies using the finite-discrete time-domain (FDTD) method by commercially available Lumerical FDTD solutions (ANSYS Inc) (for simulation details, see SI). Considering the HIL and HTLs structures, the calculated outcoupling efficiency for the device fabricated by an orientation-controlled film that has Θ = 92% was 34%. In contrast, it was 22% for the control sample made by spin-casting, which has Θ equal to 67%. Here, we computed a significant enhancement of 54.5% in the outcoupling efficiency.

To study the performance of devices, we have fabricated CQW-LEDs by SAM film of HIS NPLs and spin-coated ones as a control sample. The normalized EL spectra (see **Figure 3**c) for the device fabricated using the all-face-down orienting self-assembly (oriented-CQW-LED) and randomly-orienting spin-casting (random-CQW-LED) film of NPLs show symmetric peaks at 650 nm without any shift in the peak position. Also, efficiency graphs (see Figure 3b) illustrate a peak EQE of 16.3% for oriented-CQW-LED and 9.5% for random-CQW-LED. By comparing two devices, we detected a 71.5% enhancement in EQE. Based on our calculations, 54.5% of this improvement resulted from the enhanced light-outcoupling, and the rest 17% is attributed to the facilitated charge injection and reduced reabsorption in the case of using an ordered single monolayer of CQWs. As shown in Figure 3b, the oriented-CQW-LED device has reached its maximum EQE at lower current densities than the random-CQW-LED ones. This observation indicates the facilitated charge injection enabled by the self-assembly. Our devices are simply sealed with a glass coverslip and ultraviolet-curable resin, delivering good ambient stability. The half-lifetime (T_{50}), defined as the length of time for emitters to reach half of the initial brightness ($L_0/2$), for the oriented-CQW-LED device which was measured at the initial luminance of 5000 cd m^{-2}, was T_{50} = 89 min (see Figure 3c). Using the formula of $L_0{}^nT_{50} = L_1{}^nT$[17,36,38,48,49] and assuming an acceleration factor of n = 1.5,[17] we estimated the lifetime of 525 h at an initial luminance of 100 cd m^{-2}. Kelestemur et al.[11] reported a peak EQE of 9.92% for all-solution-processed CQW-LED using CdSe/CdS@CdZnS core/crown@HIS with a T_{50} of 560 h, and Giovanella et al.[50] reported a device with a maximum EQE of 8.39% using CdSe/CdZnS core/HIS and a peak brightness of 1500 cd m^{-2}. Thus far, our oriented-CQW-LED devices show the highest EQE among the all-solution processed CQWs. However, the maximum EQE value is still slightly lower than the record reported for CQW-LEDs.[17]

To further push the efficiency of our devices, we changed the long native ligands to shorter ones. Since the OA and OLA ligands of our as-synthesized NPLs have a very long organic tail, their length limits the charge transport rate from the carrier transport layer (CTL) to the EML, enlarging the electron-hopping distance and creating a potential barrier for energy transfer. Thus, we changed the native long OA and OLA ligands with the shorter 2-ethylhexane-1-thiol (EHT) to reduce this energy barrier for charge transport. Song et al.[38] reported a high EQE of 30.9% for red-QLED using the EHT ligands on colloidal quantum dots.

To confirm the ligand exchange, we used Fourier-transform infrared spectroscopy (FTIR) (Figure S4, Supporting

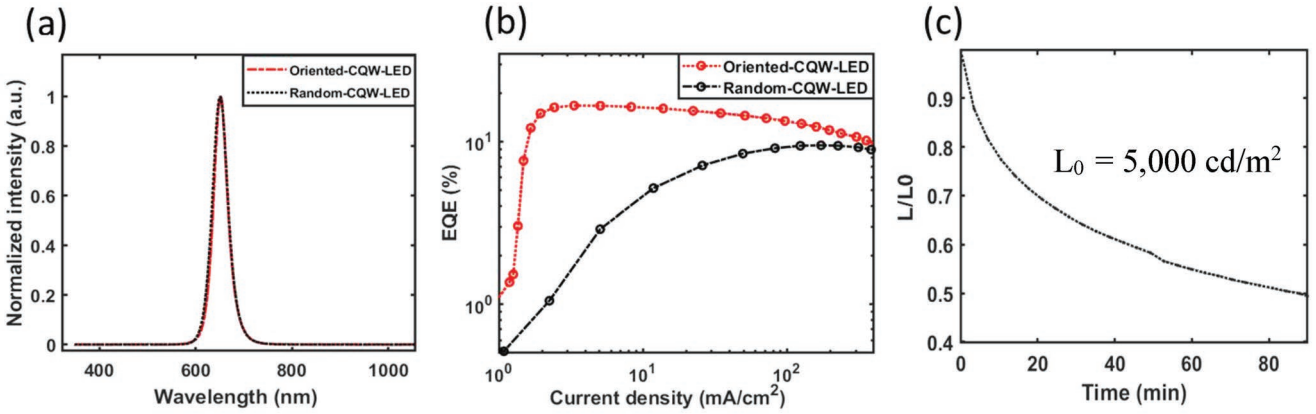

Figure 3. a) Normalized electroluminescence (EL) intensity spectra for oriented-CQW-LED and random-CQW-LED devices. b) EQE versus current density for oriented-CQW-LED and random-CQW-LED devices. c) Stability data from the oriented-CQW-LED device at the starting luminance of 5000 cd m^{-2}.

Information).[47,50] In the FTIR spectrum, the bending vibrations of the amine group of OLA (located at 1,641 cm^{-1}) of the HIS NPLs have vanished after the ligand exchange (LE-HIS samples). We found out that the ligand-exchange process affects the electrical properties of NPLs without changing the optical properties. The photoluminescence (PL) and absorption spectra for the HIS and LE-HIS samples remained unchanged (see **Figure 4**a). However, the main effect of the switch of the ligands was on the valance band position of NPLs. We measured the band offsets using the XPS technique. Here, the XPS analysis of energy bands demonstrates the effects of ligands dipole. Figure 4b illustrates the proximity of the measured E_F-E_{VBM} for NPLs with OA (0.93 eV) and EHT (1.26 eV), suggesting that the ligand exchange barely perturbs the Fermi level of NPLs. However, the main difference has been detected in the secondary electron cut-off region, indicating the ligands' dipole

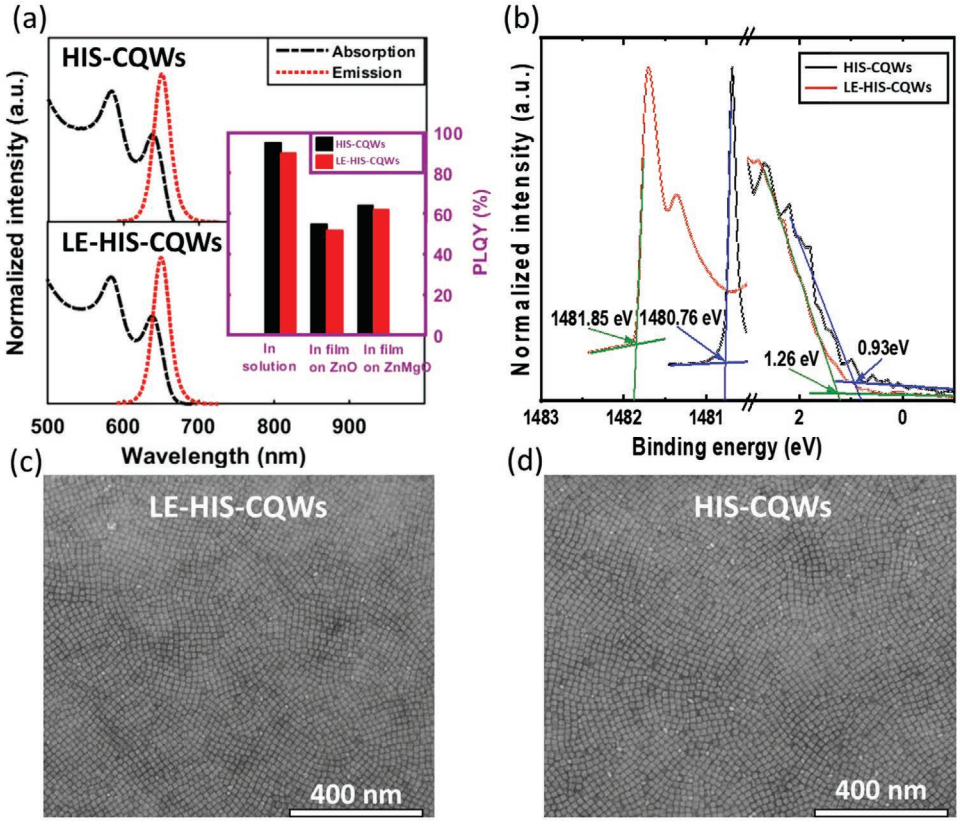

Figure 4. a) Absorption and photoluminescence (PL) spectra of the hot-injection shell (HIS) grown (top) and ligand-exchanged (LE-HIS) (bottom) CQWs. Inset, PLQY of HIS-CQWs and LE-HIS-CQWs in solution, on ZnO film and $Zn_{0.95}Mg_{0.05}O$ film. b) XPS data of second cut-off region (left-hand side) and valance band region (right-hand side). SEM images of self-assembled monolayer of c) LE-HIS-CQWs and d) HIS-CQWs on a substrate coated with the layers of ITO/PEDOT:PSS/p-TPD/PVK.

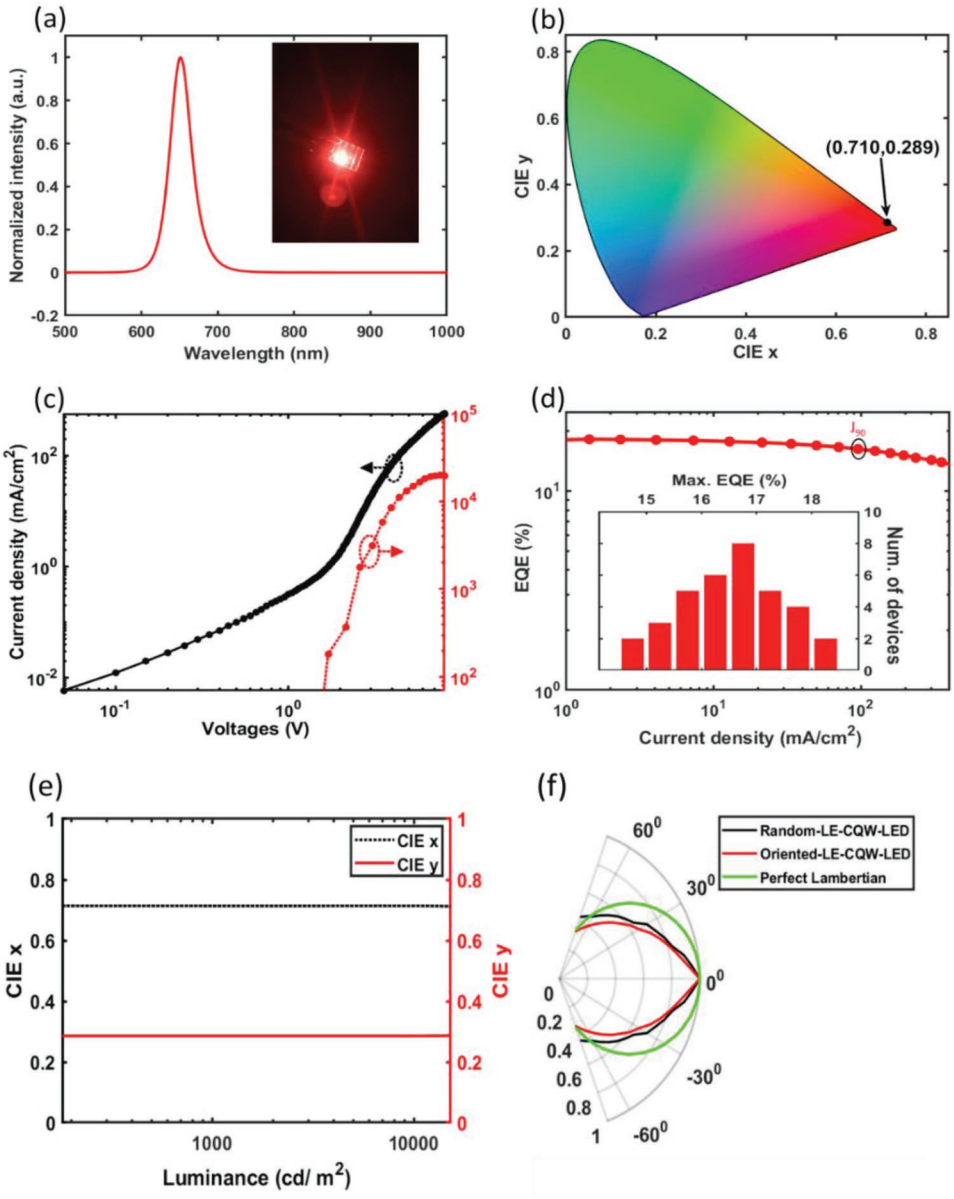

Figure 5. a) EL spectra of the LED fabricated by self-assembly and ligand exchange (oriented-LE-CQW-LED). Inset: a photograph of the device operating at 5.0 V. b) Corresponding CIE coordinates. c) Current density versus voltage and luminance versus voltages diagrams of oriented-LE-CQW-LED. d) EQE versus current density of (oriented-LE-CQW-LED) with J_{90}. Inset maximum EQE histogram of oriented-LE-CQW-LED measured from 35 devices. e) CIE coordinate as a function of the luminance. f) Emission pattern of the oriented-LE-CQW-LED, random-LE-CQW-LED devices, and that for simulated perfect Lambertian emission.

effect. Using two cut-off regions (Figure 4b) and the method of Miller et al.[52] and considering corrections,[53] the calculated E_{VBM} values were ≈5.93 for the LE-HIS samples and ≈6.61 eV for the HIS samples. Since the highest occupied molecular orbital (HOMO) of our used PVK was 5.8 eV, the potential barrier for the holes' movement from HTL to the NPLs is reduced from 0.87 eV to 0.13 eV after the ligand-exchange process.

Moreover, the EHT ligands preserve the high PLQY of the emitters. In our case, the PLQY of ensemble NPLs remained as high as 88% after the ligand exchange. Even after six times washing, the PLQY decreased only to 85%. This observation confirms the robust attachment of ligands to the NPLs by the thiol group.[38] Also, the PLQY of NPLs with and without the ligand exchange in several substrates remained close to each other (see Figure 4a). Furthermore, since the EHT ligands have a shorter length than the native ligands, the SAM film of LE-HIS NPLs is denser than the HIS NPLs. We have calculated 29×10^8 NPLs mm^{-2} and 24×10^8 NPLs mm^{-2} for the cases of LE-HIS and HIS, respectively.

The normalized EL spectrum (see **Figure 5**a) of devices fabricated use of the SAM film of LE-HIS NPLs (oriented-LE-CQW-LED) exhibits a symmetric peak at 651 nm, corresponding to a CIE coordinate of (0.710,0.289) (see Figure 5b), which is relatively close to the spectral locus of (0.708, 0.292) known

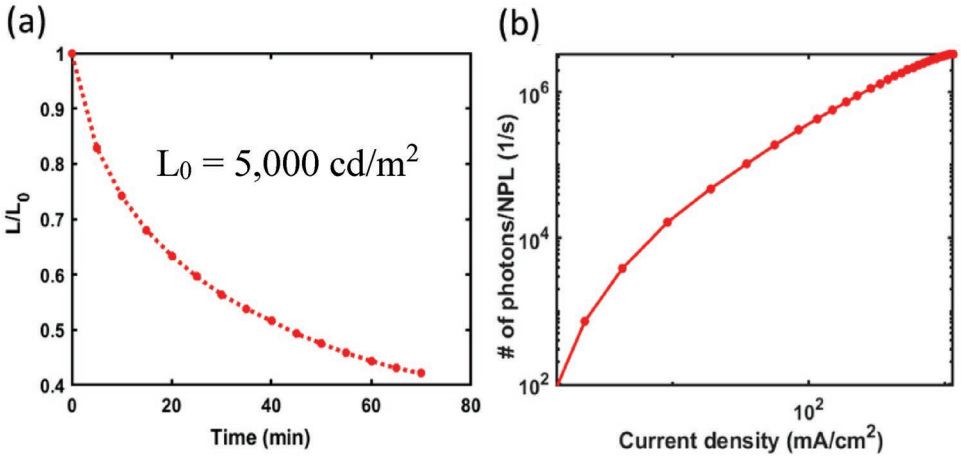

Figure 6. a) Stability data from the oriented-LE-CQW-LED device at the starting luminance of 5000 cd m^{-2}. b) Number of outcoupled photons per NPL versus current density in oriented-LE-CQW-LED.

as saturated red color. This CIE is ideal for new-generation ultra-high-definition television (UHDTV) applications.[17,38,48] The inset photograph is taken from the random-LE-CQW-LED device operating at 5.0 V. Current density-voltage and luminance-voltage (*J*–*V*–*L*) diagrams (see Figure 5c) exhibit an abrupt increase in current and luminance once they reach the sub-bandgap turn-on voltage of ≈1.7 V at a current density of 1 mA cm^{-2}, showing a typical diode behavior with a maximum brightness of 19 800 cd m^{-2} at 8.0 V. The peak EQE value of 18.1% at a current density of ≈2.36 mA cm^{-2} has been measured for these devices (see Figure 5d). This value is the highest reported EQE for all-solution processed CQW-LEDs thus far. The J_{90}, the current density in which EQE drops by 10%, is 95.58 mA cm^{-2}, which indicates outstanding stability and low-efficiency roll-off. Also, the histogram of 35 devices exhibits an average peak EQE value of 16.8%, suggesting suitable device reproducibility. Using the LE-HIS film of NPLs, we observed an 11% improvement in EQE compared to the HIS NPLs. Moreover, these devices of LE-HIS CQWs show outstanding color stability of different luminance values (see Figure 5e).

Figure 5f shows the emission patterns from a random-LE-CQW-LED and an oriented-LE-CQW-LED, along with a perfect Lambertian distribution. The oriented-LE-CQW-LED's angle of emission is narrower than that of the random-LE-CQW-LED, and both are narrower than the ideal Lambertian emission. The narrower emission profile of the random-LE-CQW-LED can be explained by the multilayered structure of our device consisting of alternating layers of materials with different refractive indices, which cause the light to be reflected and refracted at each interface, and partially acting as a waveguide to confine and guide the light within the structure. This waveguiding effect causes the light to be emitted at a specific angle, resulting in a narrow extraction cone. As a consequence of this restricted emission angle, the angular emission distribution of the randomly oriented emitters becomes narrower and approaches that of the oriented emitters in the LED device. In addition, we performed numerical computations of the device emission properties and compare our calculations with experimental measurements. Our simulation results agree with the experimental angular light intensity, validating our explanation that the angular distribution of randomly oriented emitters becomes narrower as a result of the multilayered device structure suppressing the broad-angle component of the Lambertian distribution. The calculated angular distributions of the extracted light from the LEDs with randomly-oriented emitters and orientation-controlled emitters, provided in Figure S10 (Supporting Information) along with a perfect Lambertian distribution, are in excellent agreement with the experimental results.

Our devices were simply sealed with a glass coverslip and ultraviolet-curable resin, delivering good ambient stability. The half-lifetime, measured at the initial luminance of 5000 cd m^{-2}, illustrates a T_{50} = 42 min (see **Figure 6**a). Using the formula of $L_0{}^nT_{50} = L_1{}^nT$[17,36,38,48,49] and assuming an acceleration factor of n = 1.5, we estimate the lifetime of 247 h at an initial luminance of 100 cd m^{-2}. Our reported lifetime is nineteen-fold higher than the record organic-inorganic CQW-LEDs,[17] but it is lower than the oriented-CQW-LED devices. The accumulation of charges in the EML due to shorter ligands and heating issues are considered the main reasons for this lower T_{50}.

Moreover, the self-assembled monolayer film of NPLs enables us to explore the number of generated photons per individual NPL. Since the liquid-air self-assembly yields a highly uniform ensemble film, we were able to calculate the number of NPLs inside the active region of the devices. Using SEM images (see Figure 1c) and image analysis software (ImageJ), we have found ≈13 × 10^9 NPLs inside the device's active area (4.5 mm^2). By dividing the number of nanoplatelets counted in the SEM image by the overall area of the SEM image, we obtained the density of nanoplatelets in the device. Fig 6b shows the diagram of the number of outcoupled photons per NPL versus current density. At the maximum EQE, we have ≈2180 photons/NPL per unit time. Considering the exciton lifetime of ≈10 ns in NPLs,[17,40] we have calculated ≈2 × 10^{-5} photon/NPL per unit time. However, this is the number of outcoupled photons, and to calculate the exciton number, we have computed the internal quantum efficiency (IQE) using the equation of EQE = IQE × η_{out}.[17] Since the η_{out} is 34%, we have found ≈6 × 10^{-5} exciton/NPL at a given time. This result shows that we are in the single excitonic regime in our LEDs. Also, this value at the maximum current density is ≈9 × 10^{-2} exciton/NPL, which still

is in the single exciton regime. It has been reported that for an amplified spontaneous emission (ASE), 2–5 exciton/NPL is required,[6] which is two orders of magnitude higher than the current density achieved in this study.

In conclusion, we have developed and shown highly efficient solution-processed CQW-LEDs delivering record-high EQE in the saturated red accompanied by excellent stability and a long lifetime. Such electroluminescence performance results from exploiting the orientation-controlled single monolayer film of NPLs in the EML of these devices. The use of such an oriented-NPL SAM film in the LED enables a 71.5% enhancement in the EQE compared to the randomly oriented (spin-casted) one. Also, this all-face-down NPL film yields the lowest possible surface roughness among all other deposition methods and enhances the charge injection. In addition, changing the native OA and OLA ligands with EHT leads to a densely packed film of NPLs and improves the charge injection rate (11%). By implementing the orientation-controlled film of ligand-exchanged NPLs in the devices, we obtained an EQE level of 18.1%, with a peak brightness of 19 800 cd m^{-2} in an extremely saturated red color at a CIE coordinate of (0.710, 0.289) with a T_{50} of 247 h and a J_{90} of 95.58 mA cm^{-2}. These findings demonstrate the applicability of the proposed single monolayer oriented-CQW LED architecture to fabricate high-performance all-solution-processed CQW-LEDs.

Supporting Information

Supporting Information is available from the Wiley Online Library or from the author.

Acknowledgements

H.D.B., I.B., and B.C. contributed equally to this work. The authors gratefully acknowledge the financial support in part from TUBITAK 121C266, 121N395, 120C219, 119N343, and 20AG001. B.C. acknowledges TUBITAK 2218 – National Postdoctoral Research Fellowship Program (120C219). H. V. D. also acknowledges the support from TUBA and TUBITAK 2247-A National Leader Researchers Program (121C266).

Conflict of Interest

The authors declare no conflict of interest

Data Availability Statement

The data that support the findings of this study are available from the corresponding author upon reasonable request.

Keywords

all-solution-processed light-emitting diodes (LEDs), colloidal quantum wells (CQWs), colloidal-light-emitting diodes (LEDs), orientation-controlled films, self-assembly

Received: October 25, 2022
Revised: March 6, 2023
Published online: April 6, 2023

[1] C. B. Murray, D. J. Norris, M. G. Bawendi, *J. Am. Chem. Soc.* **1993**, *115*, 8706.
[2] S. Volk, N. Yazdani, V. Wood, *J. Phys. Chem. Lett.* **2020**, *11*, 9255.
[3] S. Ithurria, D. V. Talapin, *J. Am. Chem. Soc.* **2012**, *134*, 18585.
[4] S. Ithurria, M. D. Tessier, B. Mahler, R. P. S. M. Lobo, B. Dubertret, A. L. Efros, *Nat. Mater.* **2011**, *10*, 936.
[5] S. Shendre, S. Delikanli, M. Li, D. Dede, Z. Pan, S. T. Ha, Y. H. Fu, P. L. Hernandez-Martinez, J. Yu, O. Erdem, A. I. Kuznetsov, C. Dang, T. C. Sum, H. V. Demir, *Nanoscale* **2019**, *11*, 301.
[6] Z. Chen, B. Nadal, B. Mahler, H. Aubin, B. Dubertret, *Adv. Funct. Mater.* **2014**, *24*, 295.
[7] E. Lhuillier, S. Pedetti, S. Ithurria, B. Nadal, H. Heuclin, B. Dubertret, *Acc. Chem. Res.* **2015**, *48*, 22.
[8] A. G. Vitukhnovsky, V. S. Lebedev, A. S. Selyukov, A. A. Vashchenko, R. B. Vasiliev, M. S. Sokolikova, *Chem. Phys. Lett.* **2015**, *619*, 185.
[9] S. Delikanli, O. Erdem, F. Isik, H. D. Baruj, F. Shabani, H. B. Yagci, E. G. Durmusoglu, H. V. Demir, *J. Phys. Chem. Lett.* **2021**, *12*, 2177.
[10] S. Delikanli, F. Isik, F. Shabani, H. D. Baruj, N. Taghipour, H. V. Demir, *Adv Opt Mater* **2021**, *9*, 2002220.
[11] J. Maskoun, N. Gheshlaghi, F. Isik, S. Delikanli, O. Erdem, E. Y. Erdem, H. V. Demir, *Adv. Mater.* **2021**, *33*, 2007131.
[12] N. Gheshlaghi, S. Foroutan-Barenji, O. Erdem, Y. Altintas, F. Shabani, M. H. Humayun, H. V. Demir, *Nano Lett.* **2021**, *21*, 4598.
[13] Y. Shirasaki, G. J. Supran, M. G. Bawendi, V. Bulović, *Nat. Photon.* **2013**, *7*, 13.
[14] M. Pelton, *J. Phys. Chem. C* **2018**, *122*, 10659.
[15] Y. Kelestemur, Y. Shynkarenko, M. Anni, S. Yakunin, M. L. De Giorgi, M. V. Kovalenko, *ACS Nano* **2019**, *13*, 13899.
[16] A. Polovitsyn, Z. Dang, J. L. Movilla, B. Martin-Garcia, A. H. Khan, G. H. V. Bertrand, R. Brescia, I. Moreels, *Chem. Mater.* **2017**, *29*, 5671.
[17] B. Liu, Y. Altintas, L. Wang, S. Shendre, M. Sharma, H. Sun, E. Mutlugun, H. V. Demir, *Adv Mater* **2020**, *32*, 1905824.
[18] A. A. Rossinelli, H. Rojo, A. S. Mule, M. Aellen, A. Cocina, E. D. Leo, R. Schaublin, D. J. Norris, *Chem. Mater.* **2019**, *31*, 9567.
[19] M. Sharma, S. Delikanli, H. V. Demir, *Proc. IEEE* **2020**, *108*, 655.
[20] X. Dai, Z. Zhang, Y. Jin, Y. Niu, H. Cao, X. Liang, L. Chen, J. X. P. Wang, *Nature* **2014**, *515*, 96.
[21] S. Noway, B. C. Krummacher, J. Frischeisen, N. A. Reinke, W. Brutting, *J. Appl. Phys.* **2008**, *104*, 123109.
[22] J. A. Schuller, S. Karaveli, T. Schiros, K. He, S. Yang, I. Kymissis, J. Shan, R. Zia, *Nat Nanotechnol* **2013**, *8*, 271.
[23] R. Scott, J. Heckmann, A. V. Prudnikau, A. Antanovich, A. Mikhailov, N. Owschimikow, M. Artemyev, J. I. Climente, U. Woggon, N. B. Grosse, A. W. Achtstein, *Nat Nanotechnol* **2017**, *12*, 1155.
[24] M. Sharma, K. Gungor, A. Yeltik, M. Olutas, B. Guzelturk, Y. Kelestemur, T. Erdem, S. Delikanli, J. R. McBride, H. V. Demir, *Adv Mater* **2017**, *29*, 1700821.
[25] J. Heckmann, R. Scott, A. V. Prudnikau, A. Antanovich, N. Owschimikow, M. Artemyev, J. I. Climente, U. Woggon, N. B. Grosse, A. W. Aschtstein, *Nano Lett.* **2017**, *17*, 6321.
[26] Y. Gao, M. C. Weidman, W. A. Tisdale, *Nano Lett.* **2017**, *17*, 3837.
[27] A. W. Achtstein, A. Antanovich, A. Prudnikau, R. Scott, U. Woggon, M. Artemyev, *J. Phys. Chem. C* **2015**, *119*, 20156.
[28] A. B. Vasista, D. K. Sharma, G. V. P. Kumar, *Digital Encyclopedia of Applied Physics*, Wiley-VCH, Weinheim, Germany **2019**, pp. 1–14.
[29] X. Ji, C. Chen, Y. Xiang, X. Kang, B. Shen, T. Yu, *Opt. Express* **2016**, *24*, A935.
[30] M. A. Lieb, J. M. Zavislan, L. Novotny, *J. Opt. Soc. Am. B* **2004**, *21*, 1210.
[31] H. Budde, N. Coca-Lopez, X. Shi, R. Ciesielski, A. Lombardo, D. Yoon, A. C. Ferrari, A. Hartschuh, *ACS Nano* **2016**, *10*, 1756.
[32] P. Bai, A. Hu, Y. Liu, Y. Jin, Y. Gao, *J. Phys. Chem. Lett.* **2020**, *11*, 4524.

[33] A. Lefrançois, B. Luszczynska, B. Pepin-Donat, C. Lombard, B. Bouthinon, J. Verilhac, M. Gromova, J. Faure-Vincent, S. Pouget, F. Chandezon, S. Sadki, P. Reiss, *Sci Rep* **2015**, *5*, 7768.
[34] O. Erdem, K. Gungor, B. Guzelturk, I. Tanriover, M. Sak, M. Olutas, D. Dede, Y. Kelestemur, H. V. Demir, *Nano Lett.* **2019**, *19*, 4297.
[35] Q. Yuan, T. Wang, P. Yu, H. Zhang, H. Zhang, W. Ji, *Org. Electron.* **2021**, *90*, 106086.
[36] B. Liu, S. Delikanli, Y. Gao, D. Dede, K. Gungor, H. V. Demir, *Nano Energy* **2018**, *47*, 115.
[37] H. Shen, W. Cao, N. T. Shewmon, C. Yang, L. S. Li, J. Xue, *Nano Lett.* **2015**, *20*, 47.
[38] J. Song, O. Wang, H. Shen, Q. Lin, Z. Li, L. Wang, *Adv. Funct. Mater.* **2019**, *29*, 1808377.
[39] C. Pu, X. Dai, Y. Shu, M. Zhu, Y. Deng, Y. Jin, X. Peng, *Nat. Commun.* **2020**, *11*, 937.
[40] Y. Altintas, K. Gungor, Y. Gao, M. Sak, U. Quliyeva, G. Bappi, E. Mutlugun, E. H. Sargent, H. V. Demir, *ACS Nano* **2019**, *13*, 10662.
[41] J. M. Pietryga, Y. Park, J. Lim, A. F. Fidler, W. K. Bae, S. Brovelli, V. I. Klimov, *Chem. Rev.* **2016**, *116*, 10513.
[42] Y. Altintas, U. Quliyeva, K. Gungor, O. Erdem, Y. Kelestemur, E. Mutlugun, M. V. Kovalenko, H. V. Demir, *Small* **2019**, *15*, 1804854.
[43] Y. Sun, Y. Jiang, H. Peng, J. Wei, S. Zhang, S. Chen, *Nanoscale* **2017**, *9*, 8893.
[44] H. Zhang, Q. Su, S. Chen, *Nat. Commun.* **2020**, *11*, 2826.
[45] Q. Su, H. Zhang, S. Chen, *npFlexible Electron.* **2021**, *5*, 8.
[46] L. Qian, Y. Zheng, J. Xue, P. H. Holloway, *Nat. Photon.* **2011**, *5*, 543.
[47] Z. Li, Y. Hu, H. Shen, Q. Lin, L. Wang, H. Wang, W. Zhao, L. S. Li, *Laser Photonics Rev.* **2017**, *11*, 1600227.
[48] F. Shabani, H. D. Baruj, I. Yurdakul, S. Delikanli, N. Gheshlaghi, F. Isik, B. Liu, Y. Altintas, B. Canımkurbey, H. V. Demir, *Small* **2021**, *18*, 2106115.
[49] H. V. Demir, S. Nizamoglu, T. Erdem, E. Mutlugun, N. Gaponik, A. Eychmüller, *Nano Today* **2011**, *6*, 632.
[50] U. Giovanella, M. Pasini, M. Lorenzon, F. Galeotti, C. Lucchi, F. Meinardi, S. Luzzati, B. Dubertret, S. Brovelli, *Nano Lett.* **2018**, *18*, 3441.
[51] H. Shen, W. Cao, N. T. Shewmon, C. Yang, L. S. Li, J. Xue, *Nano Lett.* **2015**, *6*, 57.
[52] E. M. Miller, D. M. Kroupa, J. Zhang, P. Schulz, A. R. Marshall, A. Kahn, S. Lany, J. M. Luther, M. C. Beard, C. L. Perkins, J. V. D. Lagemaat, *ACS Nano* **2016**, *10*, 3302.
[53] D. M. Kroupa, M. Vörös, N. P. Brawand, B. W. McNichols, E. M. Miller, J. Gu, A. J. Nozik, A. Sellinger, G. Galli, M. C. Beard, *Nat. Commun.* **2017**, *8*, 2.